CHAPTER 3: Fluorescent Gadolinium Oxide Nanoclusters

3.1 Introduction

White light emitting (WLE) nanomaterials are gaining lots of interest due to their broad applicability in the field of optical display, [298] light-emitting diodes, [299] bioimaging, [300] sensing, [301] and photo-catalysis. [302] Currently, the synthesis of WLE nanomaterials is mainly based on hybrid semiconductors (Cd, Pb), [298] carbon dots, [303] and conjugate polymers. [304] Unfortunately, heavy metal (Cd, Pb) toxicity, low emission stability, and photo blinking of organic systems are some major issues during the synthesis, which limit their real-time applicability. [305] Most importantly, using corrosive solvents, high-temperature thermal decomposition reactions, and complex ion doping methodology during the synthesis of WLE nanomaterials limits their applicability in the biomedical sector, [306] like in cellular imaging. Contrary to the above-mentioned precursors, lanthanides belong to the third group of the periodic table and have electronic configuration $4f^n5s^25p^6$, generate broad emissions ranging from UV to NIR region depending upon the variation in the exponent, [307] are appropriate for the production of WLE material. Further, the parity-forbidden transitions of 4f electronic states generate a long-duration fluorescent lifetime extremely useful for highly resolute cellular image generation with the efficacy of deep tissue penetrability. [308] The shielding effect of outer 5s and 5p orbitals also facilitates the resistance to oxidative photo-bleaching during biological usage.

Relying upon the above-discussed properties of lanthanides, gadolinium oxide (Gd_2O_3) nanosystems have been investigated broadly. The high demand for Gd_2O_3 is concerned with their single state multi efficient probe effect, which can provide large Positron Emission Tomography (X-ray attenuation coefficient smaller than Au but larger than Iodine), [309] neutron capture cross section (huge thermal neutron capture cross-section of 257000 barns),

[310] combined magnetic (high spin magnetic moment=7/2), [311] and fluorescent properties [306] in a single particle. Hence, it could be a potential material for adding white light emission. Furthermore, higher relaxation and longer circulation time (due to higher molecular weight) also make the Gd_2O_3 nanomaterial popular among other lanthanide oxides. However, for biological applications, adding white light emission from Gd_2O_3 would enable us to harness the latent capabilities of multi-fluorescent bioimaging. For further biological application, such nanosystems must be highly biocompatible and water-soluble. Previous studies have shown that despite a large contrasting cross-section of Gd_2O_3, superparamagnetic iron oxide nanoparticles (SPIONs) became a popular choice for magnetic resonance imaging (MRI) imaging agents due to biocompatibility issues in Gd_2O_3. [122] Also, on a comprehensive survey of various reports, it has been observed that, on average, Gd_2O_3 nanosystems displayed nearly 80% of cell viability, [312] majorly due to the large size of the nanoparticles. [313]

In essence, there are three challenges in this area: (i) development of single component white light emitting Gd_2O_3, which is (ii) highly biocompatible, and (iii) ultra-small in size. [298–301] Therefore, there is an urgent demand to develop white light-emitting, biocompatible, water-dispersible Gd_2O_3 nanoclusters. A broad white light spectrum would enable real-time bioimaging in the red (R), green (G), and blue (B) spectra due to extended emission in the red spectrum by Gd_2O_3 nanoclusters in the 400-800 nm region would allow easy penetration of red light radiating out of the deep tissue, resulting in higher signal to noise ratio (S/N). [314] However, investigation regarding the white light/RGB color emission from gadolinium oxides and its other polymorphs is minimal, but some recent works are being discussed here. In line with this, I Nelli et al. synthesized the Lanthanide ($Ln^{3+)}$ doped white light emitting gadolinium dioxycarbonates, [315] F.Zaman et al. synthesized the Dysprosium (Dy^{3+}) doped white light generating gadolinium borate glasses,

[316] and Murat Erdemm et al. formulated the Ytterbium / Erbium (Yb^{3+} /Er^{3+}) doped gadolinium gallium nanocrystal for white light emission. [317] Although for, acquiring multi-fluorescence capabilities has led to the development of various synthetic routes. For instance, in a slightly different approach, Shafquat et al. synthesized non-fluorescent Gd_2O_3 nanoparticles and doped them with Europium (Eu^{3+}) to obtain red color emission. [312] In another study, Mahajan et al. used a two-step elaborated process to make monodispersed 3 nm sized, red-emitting Gd_2O_3:RE^{3+} (Rare earth) nanocrystals. [318] Similarly, Zhao et al., in their research, investigated multicolour fluorescent emissions from lanthanide-doped Gd_2O_3 nanoparticles synthesized by thermal decomposition of $Gd_2(CO_3)_2$ at high temperatures. [319] Apart from lanthanide ion doping in gadolinium host lattice, researchers also adopted some complicated methods of doping carbon dots and noble metals to produce white light (RGB color) emission. [320,321] In a recent report, composite porous Gd^{3+} nanoparticles doped with carbon dots have been used to generate hyperchromic fluorescence. [322]

Moreover, there are additional challenges in view of the biological application prospects of Gd_2O_3; the development of its nano-level dimension would be a viable option for smooth internalization and renal clearance without causing additional toxicity. However, due to high interfacial energy, stabilization of sub-nanosized clusters of Gd_2O_3 poses a great challenge. This problem can be solved by choosing an appropriate template while synthesizing Gd_2O_3 nanoclusters. The templates not only help in improving the circulation of nanoclusters in the body but also enable the acquisition of a high signal-to-noise ratio ($S/N \geq 10$) during fluorescence imaging. [323] Using proteins as a template during the synthesis of nanoclusters not only improves stability but also enhances biocompatibility and water solubility. Further, due to the close proximity of capping agents with the surface of the newly developing solid sub-nano phase, the electronic stability of the core is

improved, thereby developing a broad fluorescent emission spectrum. Based on this concept, the unusual fluorescence emission from several nanoclusters has been reported. [324]

Commercially available Bovine serum albumin (BSA) protein is a popular template, [325] previously reported for imparting extraordinary stability and anomalous biocompatibility to the newly synthesized system. [325,326] Therefore, BSA was adopted as the model protein to stabilize the Gd_2O_3 clusters and provide steric protection due to the presence of 17 disulfide bonds and one free cysteine residue. [327]

Besides BSA, ascorbic acid (ASC) is a well-known water-soluble, [328] non-toxic, [313] naturally available reducing agent and could be used as an environmentally benign reducing agent when synthesizing Gd_2O_3 nanoclusters. Apart from its reducing nature, ascorbic acid holds the capability of restructuring the denatured BSA [88,329] protein probably formed during the synthesis by invading hydrophobic pockets, and thus lost fluorescent intensity can be restored. [76] Ultra-small (~2 nm) Gd_2O_3 nanoparticles were already prepared from another important organic reductant, namely citric acid, in the solution phase, but the resulting particles exhibited phosphorescence behavior in visible and NIR regions, unlike white light emission described under the current context. Further, toxic ethylene glycol was synergistically used to obtain the luminescence characteristic. [306]

Despite considerable work, white light-emitting single component-based Gd_2O_3 nanoclusters have never been reported. Current research, therefore, adopted a greener approach for developing white light-emitting, undoped Gd_2O_3 nanoclusters in the aqueous phase by employing BSA and ascorbic acid in a simple one-pot solution method. These developed nanoclusters have been examined to display tunable fluorescent emissions in the visible spectrum's blue, green, and red regions. By successfully employing the white light

emission property and RGB colors of Gd_2O_3 nanoclusters, confocal microscopic imaging of HaCaT (human epidermal keratinocytes) cell lines was realized, and the future potential of developed Gd_2O_3 nanoclusters as an efficient fluorescent probe has been established.

3.2 Experimental Section

3.2.1 Chemicals

Ultrapure deionized water was used in all experiments. 99.9% pure gadolinium (III) nitrate hexahydrate and 99.9% pure L-ascorbic acid were purchased from Sigma Aldrich, and high-quality bovine albumin serum was purchased from SRL (Sisco research laboratory) and used as received without any further purification and adulteration. DMEM (Dulbecco's modified Eagle's medium), Streptomycin, and penicillin were obtained from CELL clone™, Genetics Biotech Asia Pvt. Ltd, and Fetal bovine serum (FBS) was purchased from Gibco by Life Technologies. Trypsin-EDTA, MTT (3-(4, 5- dimethylthiazol-2-yl)-2, and 5 diphenyl tetrazolium bromide were purchased from Hi-Media. DMSO (dimethyl sulphoxide) was obtained from Merck Millipore. A tissue culture flask (surface area 25 cm^2, canted neck, vented cap) and 96 well plates (flat bottom) were purchased from Eppendorf. 12well and 6well culture plate was obtained from Genetics Biotech Asia Pvt. Ltd.

3.2.2 Synthesis of Gd_2O_3 Nanoclusters

All the glassware was washed with aqua regia ($3HNO_3$ (30%):1HCL (30%)) and rinsed thoroughly with ultrapure deionized water before starting the reaction process. In an optimal synthesis procedure, gadolinium salt (gadolinium (III) nitrate hexahydrate) (5mM/ 22.5mg) was dissolved in 10 ml ultrapure water and kept in a borosil conical flask (150 ml), followed by the addition of L- Ascorbic acid (20 mg/ml, 3 ml) into the solution and let the solution stirred for 5 min at 55 °C. Afterward, bovine albumin serum (450 mg/ml. 1 ml)

was added to the solution and kept in the reaction mixture for 2 hrs. at 55° C with constant vigorous stirring (900 rpm). Afterward, the solution was incubated at 55 °C for 72 hrs, and the changed color of the solution from colorless to light yellow, indicating the completion of the reaction process and the presence of newly formed nanoclusters.

During the entire reaction procedure, the reaction system was tightly sealed by a cotton plug and paraffin wrap to avoid oxidation and contamination from the surroundings. Furthermore, prepared particles were centrifuged using Amicon Ultra-0.5 ml to remove unreacted ligands and larger particles. Finally, washed nanoclusters with ethanol and deionized water two to three times to get rid of impurities, and then nanoclusters were re-dispersed in water and kept at 4°C until further use. In order to obtain the highly fluorescent nanoclusters, the reaction conditions were systematically optimized, and the procedure, as mentioned above, was the optimal condition. Besides, the control experiment was also performed under the same optimal condition to interrogate the fluorescence behavior of the prepared nanoclusters, and we took almost all possible controls to examine the behavioral change of fluorescence properties like (Gd^{+3} salt + BSA, Gd^{+3} salt+ Ascorbic acid, BSA + Ascorbic Acid).

3.3 Characterization

3.3.1 Transmission Electron Microscopy (TEM)

The size of fluorescent Gd_2O_3 nanoclusters was examined using a high-resolution transmission electron microscopy (HR-TEM) on an FEI Tecnai G2 20 TWIN, operating at a maximum accelerating voltage of 200 kV electron beam. For that, 10-fold diluted Gd_2O_3 nanoclusters were dropped cast onto a TEM grid, air dried at room temperature under a contamination-free environment, and observed under TEM.

3.3.2 Fluorescence Spectroscopy

The fluorescence experiment was carried out using PTI Quanta master 400, Horiba Canada spectrofluorometer (Slit width = 1 nm, integration time = 0.1s, and step size = 1nm). All the spectra of synthesized Gd_2O_3 nanoclusters and control were taken out at an optical density of less than 0.5 to avoid the inner filter effect.

3.3.3 UV-vis Spectroscopy

The UV-visible absorbance spectra of Gd_2O_3 nanoclusters (OD < 0.5) were obtained by using TestRight Prism^{+}.

3.3.4 Fourier Transform Infrared (FTIR) spectroscopy

The lyophilized Gd_2O_3 nanoclusters were mixed with KBr to make the pellets and examined with a Nicolet iS5 (THERMO Electron Scientific Instruments LLC) in 4000 to 400 cm $^{-1}$ range to obtain the FTIR spectra.

3.3.5 X-ray diffraction (XRD)

The phase and crystallinity of the lyophilized Gd_2O_3 nanoclusters were recorded using X-ray diffraction (XRD), Bruker, Model –D8 advance (Eco).

3.3.6 X-ray photoelectron spectra (XPS)

X-ray photoelectron spectra (XPS) were obtained using PHI 5000 Versa Probe III.

3.3.7 Matrix-Assisted Laser Desorption Ionization Time-of-Flight (MALDI-TOF)

MALDI-TOF analysis was performed in Bruker Autoflex speed Matrix-assisted laser desorption/ionization-time of flight facility using sinapinic acid as the matrix. The ionized (nitrogen laser of 337 nm) sample mass spectra were recorded in the positive linear mode with an average of 500 shots. The stock solution of the matrix (1 ml) was prepared by

dissolving 10 mg of sinapinic acid in a solution containing 500 µl acetonitrile and 500 µl 0.1% trifluoroacetic acid. Afterward, 1µl of 10-fold diluted Gd_2O_3 nanoclusters and 1µl of the prepared matrix were spotted onto the target plate for spotting purposes.

3.3.8 Fluorescence Life Time Decay Analysis

Average lifetime measurements of the prepared Gd_2O_3 nanoclusters and native BSA protein were carried out with Edinburgh FL920 Spectrometer using the time-resolved fluorescence spectrometer (TRFS) technique. Sample spectra were recorded at 10,000 counts by excitation of a 375 nm, 496 nm laser, and 598 LED light source. Additionally, fluorescence lifetime setups were attached to an external circulation water bath to maintain the ambient temperature at 25 °C. Furthermore, the recorded lifetime data were optimized using a tri-exponential curve to get the chi-square values near 1.00 with the help of *Decay Fit 1.4 software.*

3.3.9 Cell Culture and Cell Viability Assay

The cell viability of the HEK-293 (human embryonic kidney cell line), as well as human breast cancer cells (MDA-MB-231), was assessed while being exposed to the freshly synthesized Gd_2O_3 nanoclusters and its control (media), using an MTT dye. MTT is a colorimetric assay that is based on the conversion of the yellow tetrazolium salt MTT [3-(4, 5-dimethylthiazol-2-yl)-2, 5-diphenyl tetrazolium bromide] to purple color formazan crystals by reaction with mitochondrial succinate dehydrogenase of metabolically active cells, soluble in organic solvents like dimethyl sulphoxide (DMSO). The cell lines were incubated in complete DMEM (supplemented with 20 mM L-glutamine, 10% fetal bovine serum, 100 units/mL penicillin, and 100 µg/mL streptomycin) under 37 °C with 5% CO_2 in a humidified atmosphere. Briefly, HEK-293 and MDA-MB-231 cells were seeded in a 96-well plate at a density of 1×10^4 cells per well and incubated for 24 hrs. before adding

Gd_2O_3 nanoclusters. After 24 hrs., different concentrations of Gd_2O_3 nanocluster ($1/10^{th}$, $1/100^{th}$, $1/1000^{th}$ of 35mg/ml stock) containing fresh high glucose DMEM were incubated for 24 hrs in a 5% CO_2 humidified atmosphere in order to evaluate cytotoxic response. After 24 hrs. of incubation with a Gd_2O_3 nanocluster, the medium was replaced with 100µL of fresh medium containing 5 mg/mL MTT solution in each well, followed by incubation for 2 hrs. MTT reagent was further replaced by 100µL DMSO in each well and incubated in the dark at 37 ºC for 30 minutes to observe the formation of formazan crystals. Finally, the plates were assayed using a Micro ELISA plate reader at 570 nm. The cell viability was estimated using the following formula: -

% Cell viability = [Optical density of Gd_2O_3 treated cells/ Optical density of Control cells] ×100

3.3.10 Confocal Microscopy

The cellular uptake and fluorescence behavior of Gd_2O_3 nanoclusters was also investigated by confocal microscopy (Carl Zeiss LSM 780 confocal microscope). 2×10^4 counts of normal keratinocytes (HaCaT) cells seeded on a coverslip in 6 well culture plate. After 24 hrs. of treatment, the seeded cells were treated with a $1/10^{th}$ ratio of freshly prepared Gd_2O_3 nanoclusters (35mg/ml stock solution) with the complete medium and incubated further for 24 hrs at 37 ºC in a humidified 5% CO_2 incubator. After 24 hrs. of treatment, the media was removed, and cells were washed with PBS and fixed using 4% formaldehyde. Finally, the cells were imaged under confocal microscopy to predict their fluorescence behavior.

3.3.11 Quantum Yield Measurement

We have calculated the quantum yield of Gd_2O_3 nanoclusters in blue (366) and green (469) emissions with respect to quinine sulfate (QS) in 0.1 M H_2SO_4 and rhodamine 6G (R6G) in ethanol, respectively using with equation (1). The concentration of Gd_2O_3 nanoclusters and

references (QS, R6G) were adjusted so that their optical densities become less than 0.5 to avoid the inner filter effect.

$$q_{sg} = q_r \times \frac{i_{sg}}{i_r} \times \frac{a_r}{a_{sg}} \times \frac{{\eta_{sg}}^2}{{\eta_r}^2} \ldots\ldots\ldots\ldots\ldots\ldots (1)$$

Where,

q_{sg}: Quantum yield of samples i_{sg}: area under PL curve of sample

q_r: Quantum yield of reference i_r: area under PL curve of the reference

a_{sg}: absorbance of the sample η_{sg}: refractive index of the sample

a_r: absorbance of the reference η_r: refractive index of reference

The quantum yield of quinine sulfate and rhodamine 6G is 0.54 [330] [331], and 0.95, respectively. [332] [333]

3.4 Results and Discussion

White light-emitting Gd_2O_3 nanoclusters were prepared by the reduction of gadolinium nitrate hexahydrate in the acidic medium. Herein, a straightforward, one-pot facile synthesis has been adopted, where mixing multiple fluorescent probes or doping of rare earth material has been completely avoided. In order to obtain white light emitting Gd_2O_3 nanoclusters, metal salt was reduced and stabilized in the solution with the help of non-toxic ascorbic acid and BSA protein, respectively (Discussed in section 3.2). Moreover, due to the small size and steric protection of Gd_2O_3 by BSA, it could be safely utilized in the biological system and retained for longer. [325] [334] The BSA protein is well known to serve as a template for controlled nucleation and grain growth of nanoclusters, imparting colloidal stability, [335] and the commercially available ascorbic acid was used as a reductant, which is non-toxic and biodegradable [336] in nature. It has been observed that fluorescence intensity in longer wavelengths (green, red) increases (Figure 3.1) with

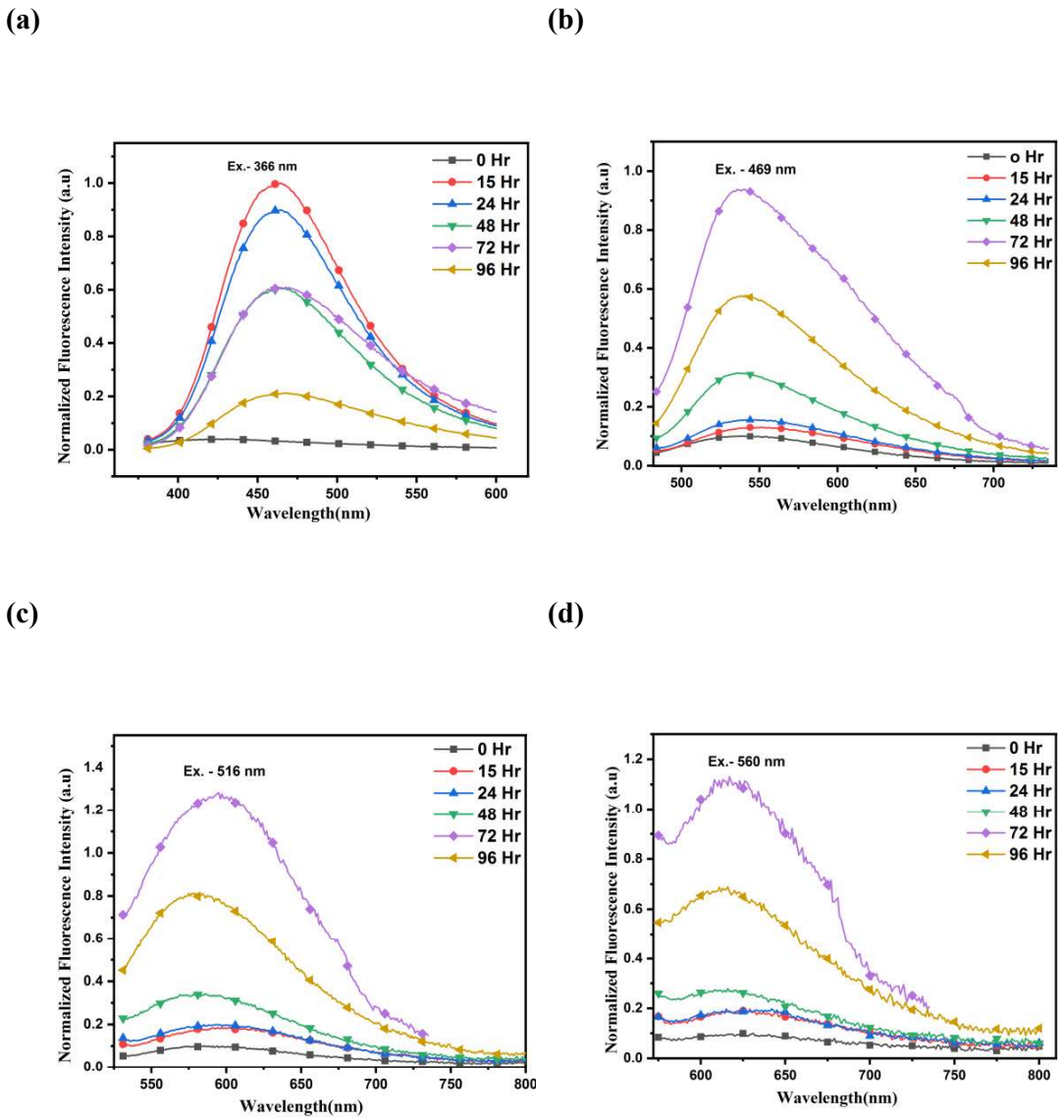

Figure 3.1: Optimization of incubation time at 0 hr, 15 hrs, 24 hrs, 48 hrs, 72 hrs, and 96 hrs of the Gd_2O_3 nanoclusters at particular excitation of (a) 366 nm, (b) 469 nm, (c) 516 nm, and (d) 560 nm.

incubation time (up to 72 hrs.) due to the formation of a larger nanocluster, which is in good harmony with other published articles. [337]

The fluorescence properties of control-1 (Gd salt + BSA), control-2 (Gd salt + Ascorbic acid), and BSA-encapsulated Gd_2O_3 nanoclusters were ascertained by acquiring fluorescence spectra, as shown in Figure 3.2. The fluorescence spectra for each sample

were acquired by exposing the sample to the 366 nm, 469 nm, 516 nm, and 560 nm light sources and observing the emission. Gd_2O_3 nanoclusters fluoresced in blue (465 nm), green (546 nm), yellow (595 nm), and red (615 nm) regions at the above excitations, respectively. (Figure 3.2) On the contrary, no significant fluorescent emission in red and green channels was observed from control 1 and control 2. However, weak fluorescence emission in blue was observed in controls 1 and 2 (Figure 3.2 (a)), which could be due to endogenous fluorescence of tryptophan residue (BSA) [60,338] and oxidation of ascorbic acid to dehydroascorbic acid, which reduce the Gd^{+3} salt into Gd^{+2} and form Gd-ascorbic complex. [339]

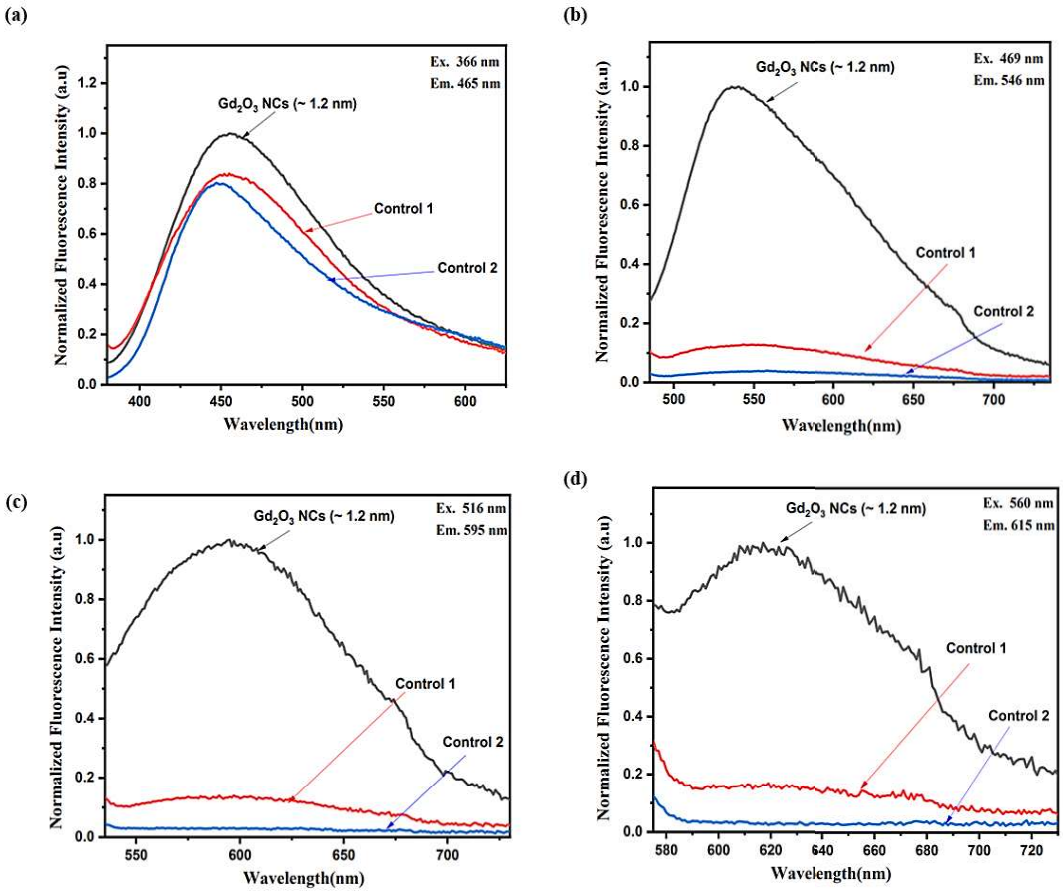

Figure 3.2: The fluorescence emission spectra of Gd_2O_3 nanoclusters and its controls (Gd salt + BSA) and (Gd salt + ascorbic acid) (a) The optimal excitation-emission spectra of Gd_2O_3 nanoclusters and controls at Ex- 366 / Em- 465 (b) The optimal excitation-emission spectra of Gd_2O_3 nanoclusters and controls at Ex- 469 / Em- 546 (c) The optimal excitation-emission spectra of Gd_2O_3 nanoclusters and controls at Ex- 516 / Em- 595 (d) The optimal excitation-emission spectra of Gd_2O_3 nanoclusters and controls at Ex- 560 /Em- 615.

Note that the ascorbic acid and BSA were also used as one of the controls during this study, and it was observed that, after 72 hrs. of incubation, it turned into an unstable dark brown solid. Hence, no further investigations could be performed on this control. Moreover, the origin of fluorescence in nanoclusters is still debatable among several hypotheses. However, the two hypotheses attained more scientific consensus: (i) location-independent, trap-assisted emission of exciton and (ii) location-dependent different emission state of

exciton. [303] Here, it is anticipated that the fluorescence that ensued from Gd_2O_3 nanoclusters could be due to electronic transition at the C=O, C-N functional group (BSA), covalently attached on the passivated surface of Gd_2O_3 nanocluster, [304][303] which can be further supported by FTIR and lifetime studies. This broad spectral emission from the Gd_2O_3 nanoclusters can be easily employed in bioimaging or photo-assisted therapies. [306] [340]

Further, the fluorescence emanating from Gd_2O_3 nanoclusters was characterized by broad spectra spanning from 400-615 nm with full-width half maxima (FWHM) of ~140 nm (Figure 3.3 (a)). The broad spectrum yielded a color chromaticity index coordinate of (0.33, 0.37), which can be attributed to pure white light (Commission Internationale de l'Elcairage (CIE) – 0.33,0.33) [315,341] (Figure 3.3 (b)). It is important to note that, so far, most of the known routes have adopted two methods: (i) optimized mixing of red, green, and blue light-emitting dye together to obtain WLE material, [59] and (ii) doping of rare earth metals like Er^{3+} and Yb^{3+} to different hosts using the different synthetic methods. [342] [343] However, the current study has employed a simple, affordable, non-toxic, green synthetic route to obtain WLE from a single material, a unique feature. Although, the nature of the luminescence emission by nanoclusters is still evolving. Among different theories, (i) emission from the core and (ii) emission from ligand shell due to metal-to-ligand or ligand metal charge transfer have been widely acclaimed as the primary reasons for such anomalous emission. [344] [325] To further investigate these two plausible theories, fluorescence lifetime and UV-visible spectroscopy studies were performed.

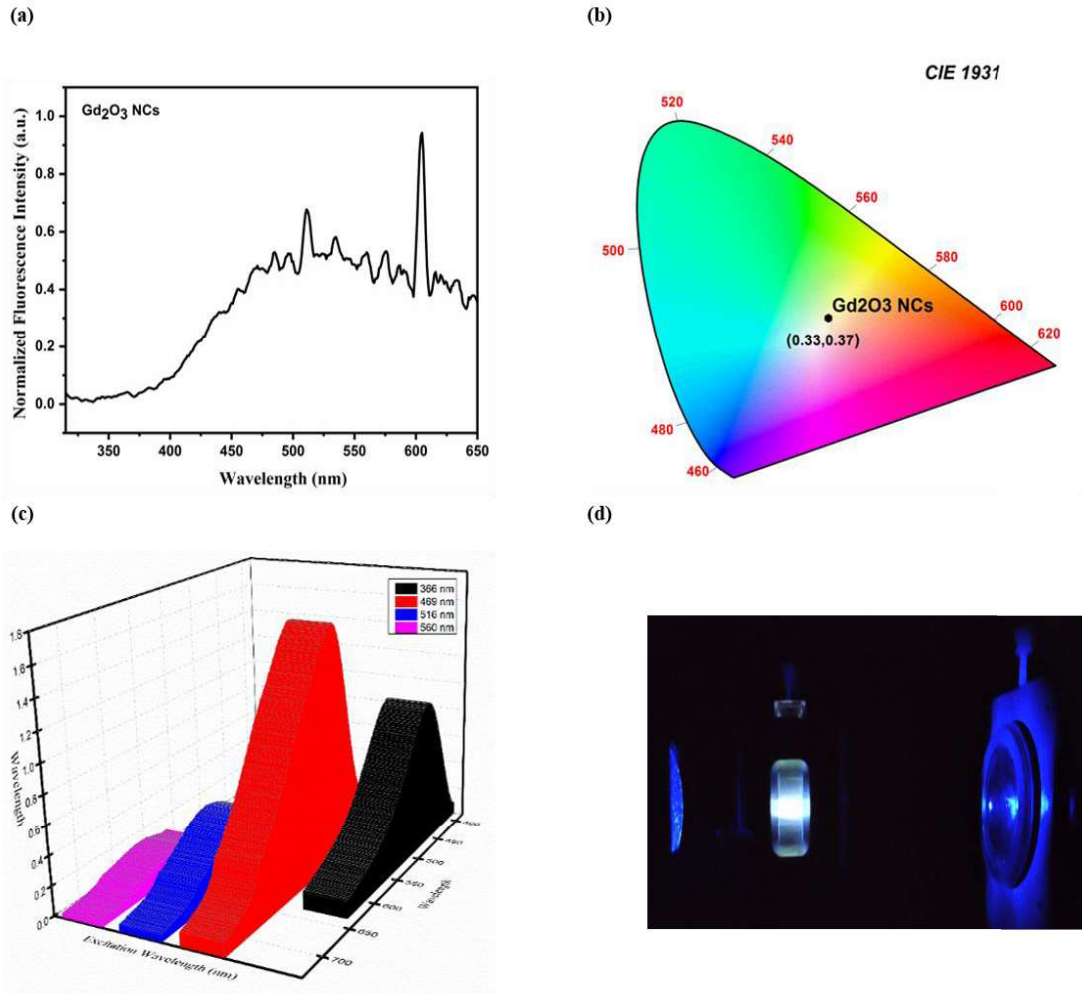

Figure 3.3: (a) Normalized fluorescent spectra of Gd_2O_3 nanoclusters at excitation 300 nm, (b) CIE 1931 chromaticity diagram for Gd_2O_3 nanoclusters with coordinate (0.33,0.37) which nearly by ideal white light coordinate (0.33,0.33), (c) Excitation wavelength dependent normalized 3D fluorescent intensity spectra, (d) White light Emission of Gd_2O_3 nanoclusters under excitation.

Initially, lifetime measurements were performed over Gd_2O_3 nanocluster samples only since other samples did not display any significant fluorescence. Fluorescence lifetime measurements were performed on the Gd_2O_3 nanoclusters and incubated BSA, corresponding to 375, 496, and 598 nm excitation. (Figure 3.4 & Figure 3.5). Fitted data indicated an average lifetime for incubated and processed BSA as 5.38 ns, 4.08 ns, and 0.15

ns, whereas nanoclusters displayed an average lifetime of 3.99 ns, 3.22 ns, and 0.52 ns, respectively. (Table 3.1)

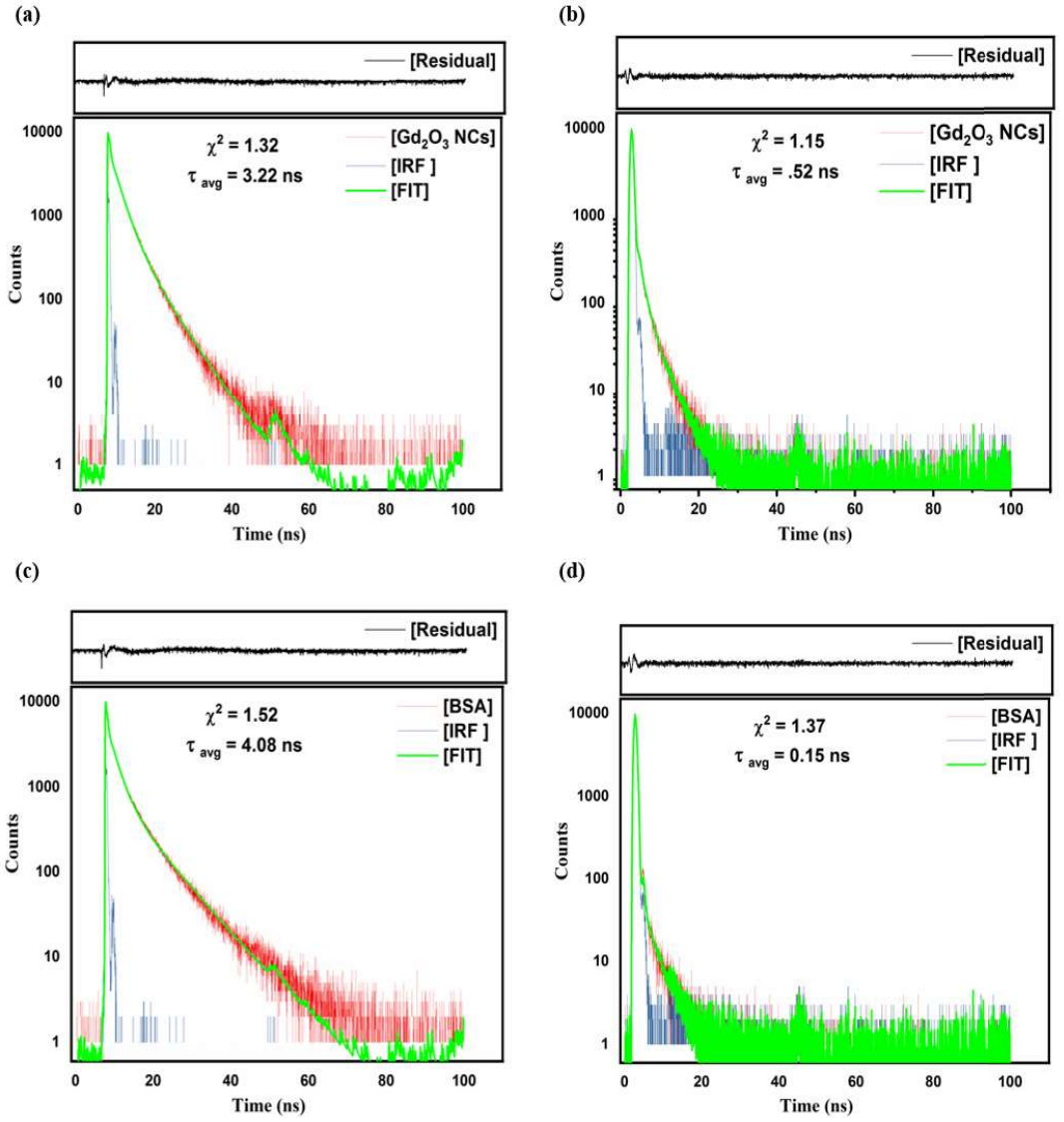

Figure 3.4: Fluorescent intensity decay lifetime spectra of Gd_2O_3 nanoclusters with IRF (Instrument response function) (a) Ex- 496 nm / Em- 564 nm, (b) Ex- 598 nm /Em- 658 nm. Fluorescent intensity decay lifetime spectra of incubated BSA (c) Ex- 496 nm /Em- 564 nm, (d) Ex - 598 nm / Em- 658 nm.

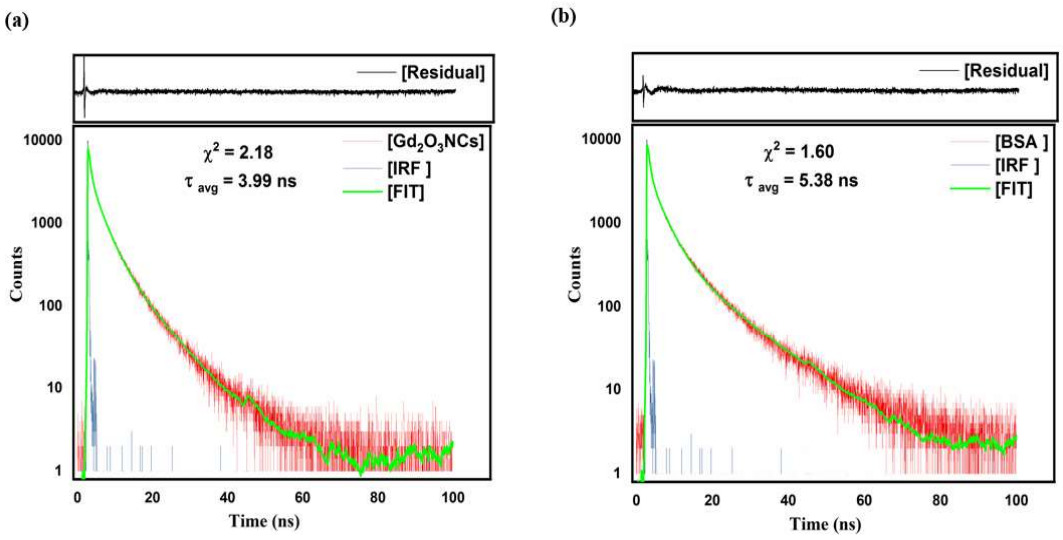

Figure 3.5: (a) Lifetime decay spectra for Gd_2O_3 nanoclusters (Ex. - 375 nm; Em. - 459 nm), (b) Lifetime decay spectra for BSA protein (Ex. - 375 nm; Em. - 459 nm).

Table 3.1: Fluorescence lifetime of Gd_2O_3 nanoclusters and incubated BSA

x	α_1	τ_1 (ns)	α_2	τ_2 (ns)	α_3	τ_3 (ns)	τ_{avg}	$\chi 2$
Blue Gd_2O_3 NCs	0.62131	0.55765	0.06233	8.20913	0.31636	2.95444	3.99	2.1
Green Gd_2O_3 NCs	0.67177	0.22391	0.05412	6.15904	0.27411	2.42166	3.22	1.3
Red Gd_2O_3 NCs	0.99608	0.02913	0.00080	3.67934	0.00312	1.56169	0.52	1.1
BSA[1]	0.63805	0.60632	0.05063	11.9412	0.31133	3.37376	5.39	1.6
BSA [2]	0.21679	2.28863	0.04166	8.26922	0.74155	0.18933	4.09	1.5
BSA [3]	0.00000	0.47549	0.00033	2.93256	0.99967	0.02158	0.15	1.3

$BSA^{1,}$ BSA^2, and BSA^3 coincide with the excitation of 375 nm laser (blue emission), 496 nm laser (green emission), and 598 nm LED lamp (red emission), respectively.

An average lifetime was calculated with equation (2).

$$T_{avg} = \frac{\alpha_1 t_1^2 + \alpha_2 t_2^2 + \alpha_3 t_3^2}{\alpha_1 t_1 + \alpha_2 t_2 + \alpha_3 t_3} \quad \text{..... (2)}$$

Where T_{avg} is the average lifetime. $\chi 2$ represents the range of fitting between the model and experimental data.

It is important to note that the average lifetime from incubated BSA is always higher than nanoclusters except at 598 nm excitation. This data indicates that at higher excitation energies, the luminescence process is dominated by the ligand-to-core charge transfer, [345] which is also evident in the UV-visible spectra (Figure 3.6 (a)). Further, the UV-visible spectra indicated a hypochromic spectral shift in nanoclusters with respect to the BSA by at least ~20 nm. It is clearly observed that the characteristic absorbance peak of BSA centred at 280 nm (due to aromatic residues and disulfide bond) [346][170] is shifted to 261 nm in the case of nanoclusters, which can be attributed to a change in the electronic environment around the amide bond (BSA) and formation of new species. [347] Additionally, it is important to note that the absence of an absorbance peak in the range of 400-800 nm wavelength indicates the formation of ultrafine nanoclusters. [344] [348] However, in the case of low-energy excitations, the lifetime of nanoclusters is slightly higher than the BSA lifetime, possibly due to weak charge stabilization from the local low-energy traps formed over the nanocluster surfaces during the synthesis. In essence, UV-visible spectroscopy confirmed the formation of ultrafine nanoclusters, change in an electronic environment, and electron transfer from ligand to the core of the nanoparticles, justifying the short lifetime visible in most of the cases except emission in the red spectrum. Further, lifetime and absorbance studies indicated ligand-to-metal charge transfer as a plausible luminescence mechanism in the nanocluster.

The TEM analysis revealed the formation of ultra-fine uniform-sized spherical nanoclusters. The average diameter of particles was calculated (*ImageJ* software) to be 1.25±0.5nm using 200 nanoclusters. The average size distribution curve showed Gaussian distribution (Figure 3.6 (b) (inset 3.6 (b)). Further, MALDI-TOF analysis was performed on BSA protein as a marker and Gd_2O_3 nanoclusters to ascertain the number of atom clusters involved in the formation, as shown (Figure 3.6 (c, d)). This MALDI-TOF analysis indicated two sharp peaks corresponding to the m/z ratio of 66418 Dalton and 66966 Dalton attributed to BSA and fluorescent Gd_2O_3 nanoclusters. Based on molecular weight offset with respect to BSA protein, the number of Gd atom nanoclusters associated with fluorescent Gd_2O_3 was found to be nearly two. It is essential to point out that using the TEM analysis, three atomic Gd_2O_3 nanoclusters were mathematically calculated, which is very close to the predicted value by MALDI-TOF. Furthermore, the composition of the fluorescence nanocluster was assessed by X-ray diffraction (XRD) and X-ray photoelectron spectroscopy (XPS).

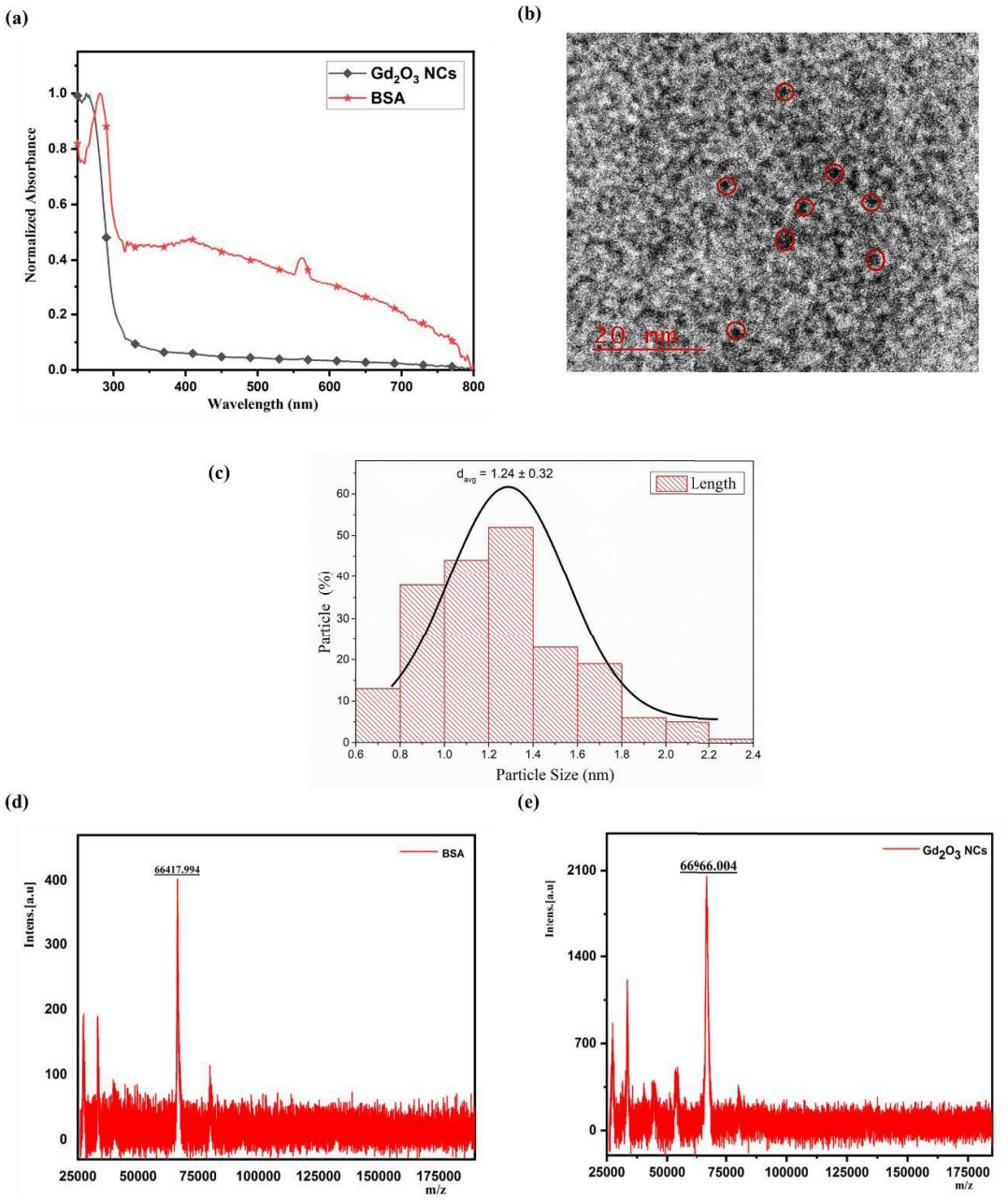

Figure 3.6: (a) UV spectroscopy of Gd_2O_3 nanoclusters and native BSA. (b) HR-TEM image of Gd_2O_3 nanoclusters, (c) The histogram distribution plot for Gd_2O_3 nanoclusters, where d_{avg} is the diameter average, (d), (e) Maldi-Tof spectra of BSA protein and Gd_2O_3 nanoclusters, respectively.

Initially, XRD spectra of BSA and fluorescence nanoclusters were acquired. (Figure 3.7 (a)) shows three broad diffraction peaks at 9°, 20°, and 29.5°, attributing to intermolecular H-bonding between the protein chains of BSA, thereby displaying its crystalline nature. [349] Notice that the XRD pattern of BSA caped fluorescence nanoclusters displayed only two distinct diffraction peaks at 20° and 29.5°, which was similar to the XRD pattern of the native BSA, while the lower peaks (9°) vanished or decreased in the intensity due to increase in the degree of bonding between protein chain and nanoclusters and hence decreasing BSA crystallinity. [350] [351] However, the XRD pattern failed to provide detailed compositional information about the nanoclusters, probably due to forming a pre-nucleating ultra-fine nanocluster. However, crystallinity exhibited by the fluorescence nanoclusters may have resulted due to the BSA only. [350] These observations confirmed that BSA was homogenously capped into the nanoclusters. [344] Therefore, to obtain detailed composition and oxidation state of fluorescence, nanoclusters were investigated using XPS, followed by FTIR analysis.

The XPS survey data of Gd_2O_3 nanoclusters are displayed in Figure 3.7 (b), which were corrected and deconvoluted with respect to the C1s spectrum shown in (Figure 3.8 (a)). The deconvoluted spectra showed two distinct peaks at 284.2 and 284.4, indicating sp^2 hybridized hydrocarbon, whereas the peak at 287.4 eV corresponds to the carbonyl compound present in BSA protein associated with Gd_2O_3 nanocluster. [352,353] Furthermore, the 4d spectra of Gd displayed (Figure 3.7 (c)) two intense peaks at 147.8 eV and 141.8 eV, indicating 4d 3/2 and 4d 5/2 energy levels of Gd, respectively. [142,354,355] Whereas the additional peak at 144.0 eV was attributed to the +3-oxidation state of gadolinium and indicated the formation of Gd_2O_3 nanoclusters. [356] While O 1s spectra (Figure 3.7 (d)) showed two clear peaks at 531.05 eV and 531.9 eV, corresponding to the bond between O^{2-} and Gd^{3+} and later peak (531.9 eV) could be assigned to double bounded

oxygen in the carboxylic group of the protein associated with Gd_2O_3 nanocluster [357],[358]. These results harmonize with previously published XPS studies on gadolinium oxide nanoclusters. [359] [306] [360]

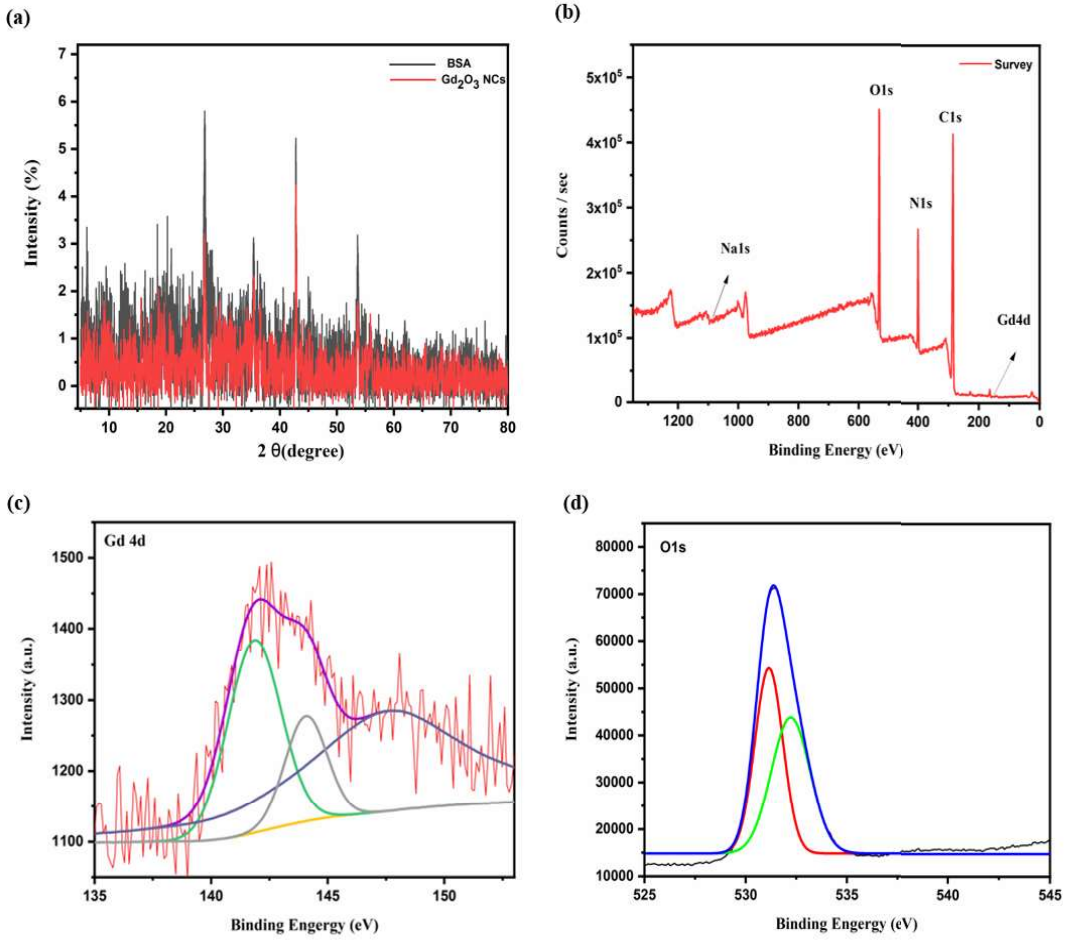

Figure 3.7: (a) HR- XRD of Gd_2O_3 nanoclusters and native BSA. Full resolution XPS data (b) Survey data. (c) Gd4d, (d) O1s.

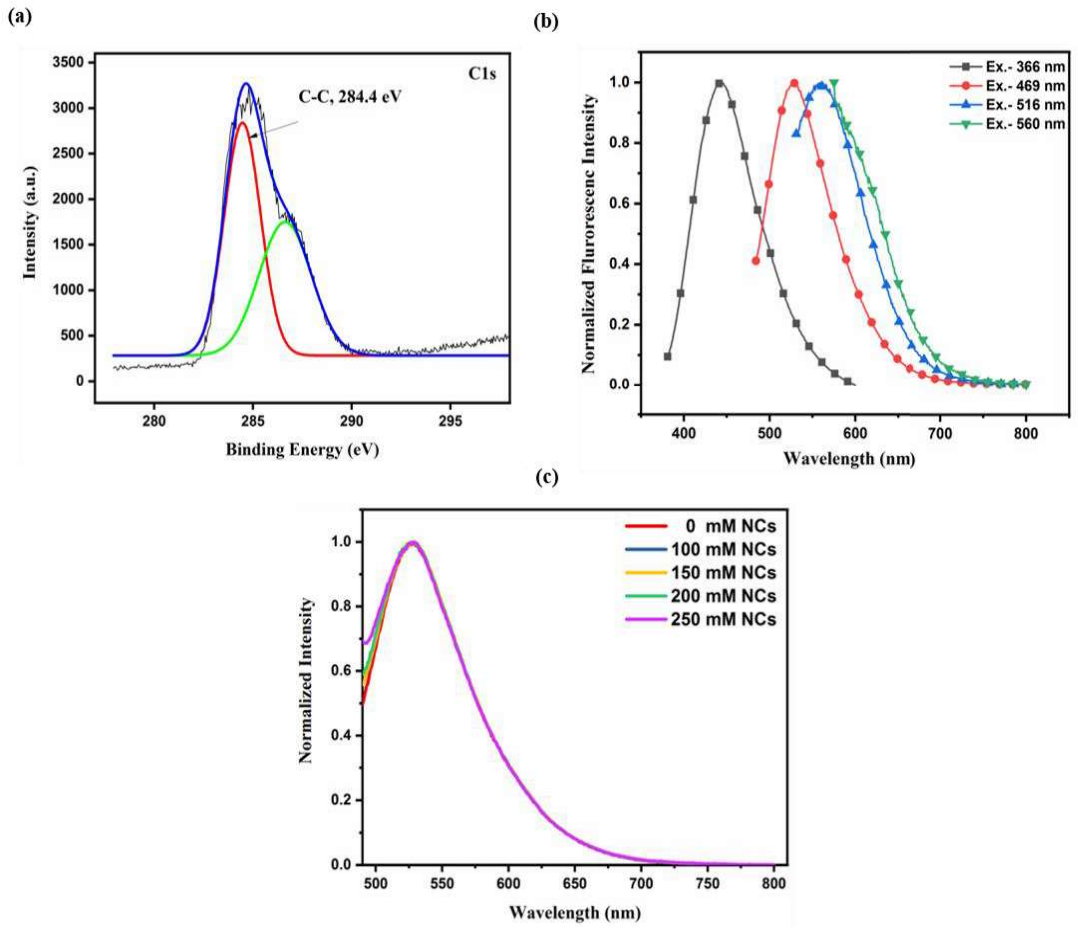

Figure 3.8: (a) XPS spectra of C 1s. (b) Fluorescence emission spectra of lyophilized Gd_2O_3 nanoclusters powder at different excitations of 366 nm, 469 nm, 516 nm and 560 nm. (c) Fluorescence emission spectrum of Gd_2O_3 nanoclusters at excitation of 516 nm after addition of freshly prepared NaCl at different concentrations of solution.

It is important to note that XPS results were also in accordance with FTIR results. The detailed FTIR analysis was performed on BSA and Gd_2O_3, as shown in (Figure 3.9 (a)). The FTIR data showed amide bands ranging from 1600-1700 cm^{-1}, 1480-1575 $cm^{-1,}$ and 1229-1301 cm^{-1} assigned to C=O stretching, N-H bending coupled with C-N stretching and C=O bend coupled with C=C stretching respectively, associated with BSA protein. Also, prominent peaks at 3400-3000 cm^{-1} comprise –NH and –OH stretching of the BSA. [325,361,362] A significant reduction in the amide peak intensities was observed due to the interaction of Gd^{+3} ion with C=O, N-H, and C-N groups of BSA protein as per the

HSAB (Hard and soft acid base) binding Lewis's theory. [363] The binding of Gd^{+3} ion with C=O and C-N functional groups of BSA protein was further evidenced by a spectral shifting of amide I (1654→1655) and amide II (1539→1540) bonds. Additionally, the shifted amide "A" band (of protein) (3304 →3291) relates to the interaction of the Gd^{+3} ion with the C-N functional group of protein, [364] which plays a crucial role in fluorescence origin. [337,365,366] The XPS and FTIR analysis strongly supports the formation of BSA-encapsulated Gd_2O_3 nanoclusters. In essence, our studies so far have proved the formation of pre-nucleating BSA-encapsulated Gd_2O_3 nanoclusters. However, the fluorescent stability of the pre-nucleating nanoclusters and parameters related to their applications also need to be investigated.

Fluorescence stability of the pre-nucleating nanoclusters was observed in the aqueous suspensions (Figure 3.10 (a, b)) stored at ~pH 4 and 4 °C for over 2.5 years. Interestingly, the emission spectra (Ex: 469 nm, and Em: 540 nm) of Gd_2O_3 nanoclusters after 7 days were found to be 10% less intense than the 2.5-year sample. At the same time, 2.5-year samples fluoresced at ~595 nm, ~20% more intense than the 7-day samples.

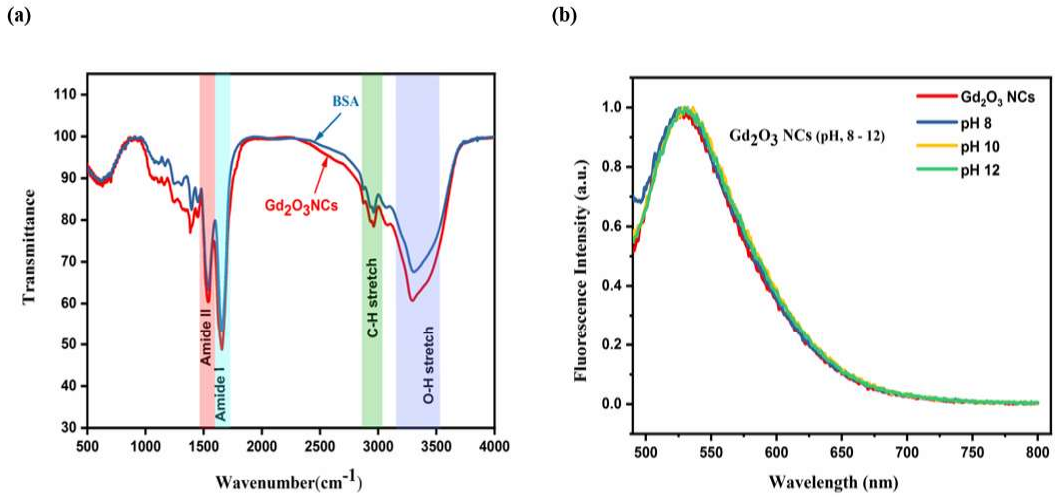

Figure 3.9: (a) FTIR Spectra of Gd_2O_3 nanoclusters, (b) pH stability fluorescent spectra at various pH (8, 10 and 12).

Furthermore, it was also observed that the fluorescence spectra of the lyophilized samples exhibited identical characteristic spectra as a colloidal sample, even after more than a year (Figure 3.8 (b)). Indicating the formation of highly stable nanoclusters, even in powder form, thus can be easily stored in any phase and used whenever required. The stability and solubility of prepared clusters are totally governed by the capping agents. In our studies, we used BSA protein as a capping ligand, which is rich in -SH, -NH_2, and -COOH functional groups. FTIR spectra also suggested the surface modification of Gd_2O_3 nanoclusters via the covalent attachment of -NH_2, COOH functional groups owning exceptional stability and higher solubility in aqueous medium. Meanwhile, ionic strength (ranging from 0 mM to 250 mM) was measured by adding the nanoclusters to the saline solution (Figure 3.8 (c)), no significant change in fluorescence intensity occurred. These studies show excellent stability of nanoclusters in both acidic and alkaline mediums in addition to a wide range of ionic strength.

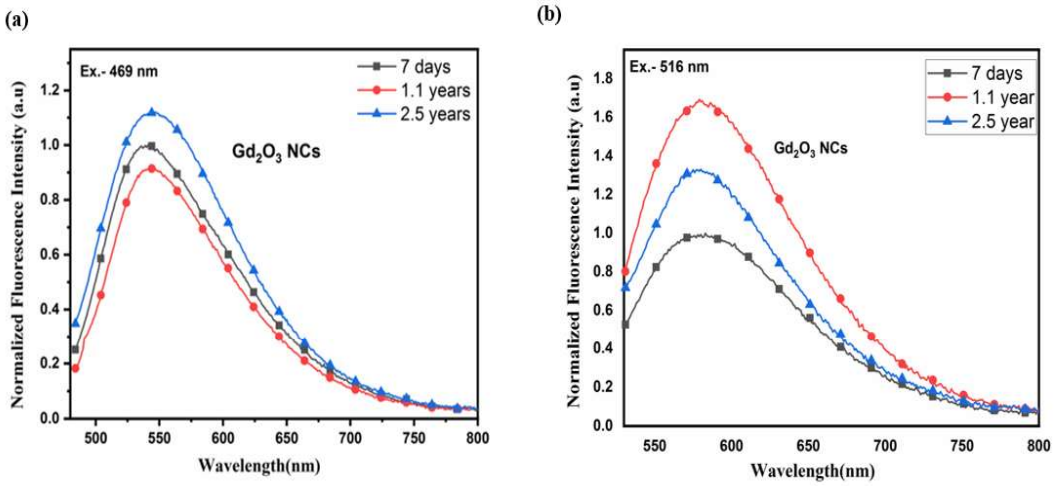

Figure 3.10: (a) Fluorescence emission spectra of Gd_2O_3 nanoclusters (Conc. 11.6 mg/ml) at excitations of 469 nm at different time intervals of 7 days, 1.1 years and 2.5 years show very eminent emission. (b) Fluorescence emission spectra of Gd_2O_3 nanoclusters (Conc.11.6 mg/ml) at excitations of 516 nm at different time intervals of 7 days, 1.1 years and 2.5 years show very eminent emission.

3.4.1 Applications of Gd_2O_3 Nanoclusters

Initially, band gap studies over the WLE Gd_2O_3 nanoclusters were assessed. The direct optical band gap (DOBP) and indirect optical band gap (IOBP) have been computed from the Tauc plot by plotting $(ahv)^2$ versus hν (Figure 3.11 (a, b)). Where α = absorption coefficient, h = Plank constant, ν = photon frequency. This plot yielded a direct band gap of 5.32 eV and an indirect band gap of 5.08 eV, which is in good agreement with other published reports on fluorescent Gd_2O_3. [312,367,368] Early studies suggested the relation of band gap with a degree of structural changes within the lattice is a phenomenon that leads to a change in the energy level distribution within the optical band gap of nanomaterial. [369]

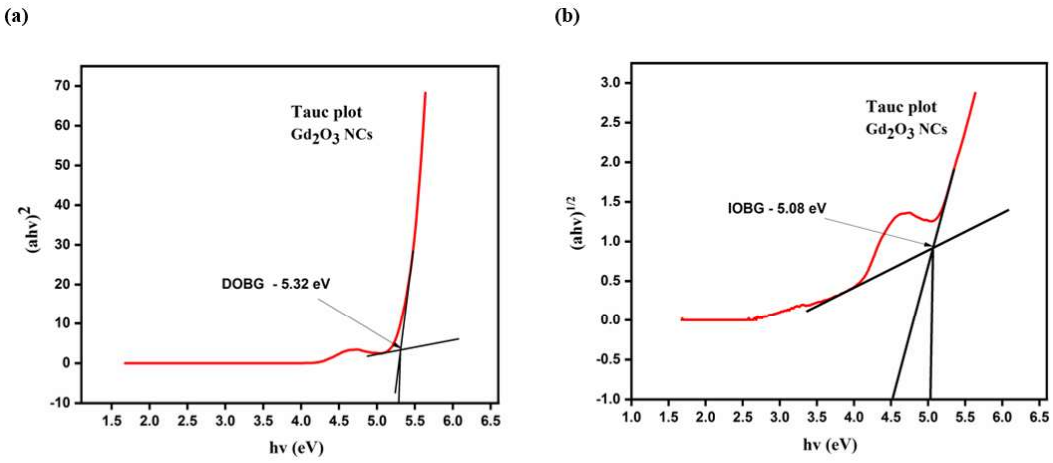

Figure 3.11: (a) Plot for Direct optical band gap of Gd_2O_3 nanoclusters between $(\alpha hv)^2$ vs. (hv), (b) Plot for Indirect optical band gap of Gd_2O_3 nanoclusters between $(\alpha hv)^2$ vs. (hv).

Next, the relative quantum yield of the nanoclusters was evaluated using quinine sulfate and rhodamine 6G as reference dyes in the blue and green regions, respectively. [370] It was observed that BSA capped WLE Gd_2O_3 nanocluster fluoresced in the blue and green region with a quantum yield of 1.85 % and 4.6%, respectively (Figure 3.12 (a, b)). In addition to quantum yield, the photo-stability of the WLE Gd_2O_3 nanocluster was

evaluated. Often, the fluorescent labels tend to temporarily/permanently lose their property under strong fluorescence excitation due to saturation or permanent change molecular structure of the molecule, leading to poor image quality. Therefore, under intense light exposure, time-based studies were performed over the nanoclusters, and its emission with time (1.5 hrs.) was acquired (Figure 3.12 (c)). Time-based studies displayed stable emission from Gd_2O_3 nanoclusters at almost all the wavelengths with ±5% variation in intensity, indicating its potential to serve as a fluorescent label for bioimaging. However, for a high signal-to-noise ratio bioimages, the quantum yield of Gd_2O_3 needs to be ascertained, along with its biocompatibility (MTT), to ensure the vitality of the cell lines. The effect of Gd_2O_3 nanoclusters on the viability of the breast cancer cell line (MDA-MB-231) as well as the standard cell line (HEK-293) was assessed by MTT assay (Figure 3.13 (a, b)). The MTT assay on Gd_2O_3 incubated cell lines, HEK-293 and MDA-MB-231, displayed as little as 6% loss in viability for $1/10^{th}$ the dilution of nanoclusters (stock solution = 35 mg/mL). This mortality of cells further decreased to 1% when the dilution of Gd_2O_3 was increased to 1/100 in the case of HEK-293. While in the case of MDA-MB-231 cell lines, for the same dilution of Gd_2O_3, the viability of cell lines dropped by 8% and 2%, respectively, when compared to their respective controls. The low toxicity might have resulted due to rigid confinement of Gd^{+3} in BSA-caped Gd_2O_3. Early studies by Shafquat Majeed et al. suggested that the low toxicity of nanocrystals is due to the agglomeration of nanoparticles [312].

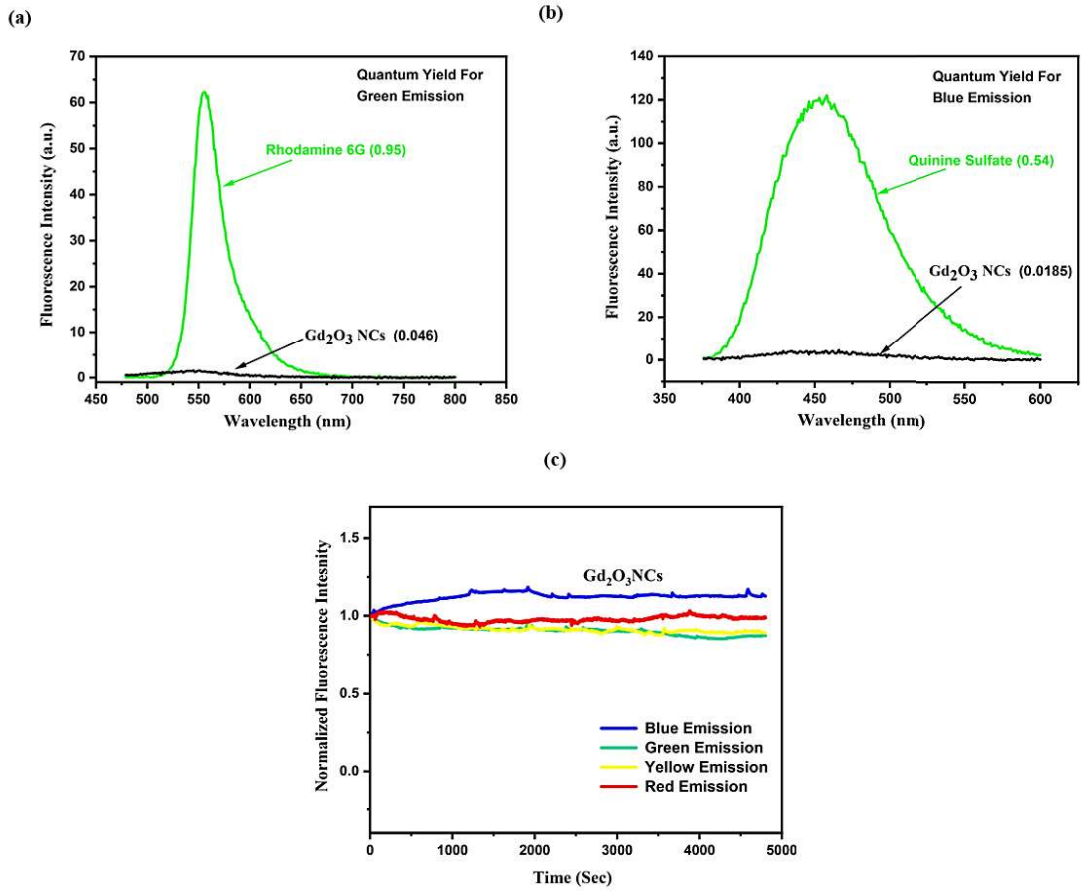

Figure 3.12: (a) Quantum yield for green emission of Gd_2O_3 nanoclusters with rhodamine 6G as a reference at the same absorbance (≤0.5), (b) Quantum yield for blue emission of Gd_2O_3 nanoclusters with quinine sulfate as a reference at same absorbance (≤0.5). (c) Photo-stability of Gd_2O_3 nanoclusters for different excitations 366,469,516 and 560 nm.

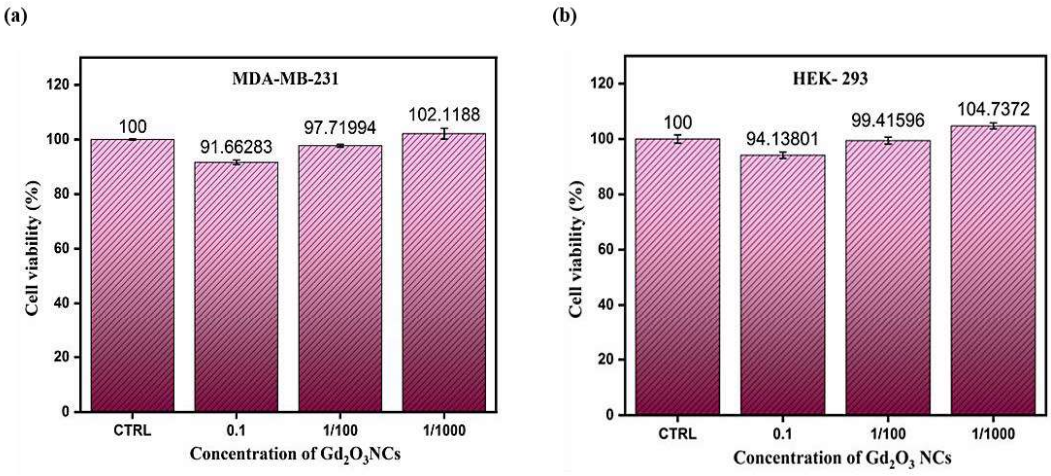

Figure 3.13: (a) and (b) Percentage cell viability: MTT assay histogram of Gd_2O_3 nanoclusters on MDA-MB -231 and HEK-239 treated with different concentrations, respectively, (Stock concentration 35 mg/ml)

3.4.2 *In-vitro* imaging of Gd_2O_3 in HaCaT cell line

Apart from the cell viability assay, the live cell bioimaging in the HaCaT cell lines was also performed using confocal laser scanning microscopy (Figure 3.14). Microscopic image of Gd_2O_3 nanocluster incubated HaCaT cells revealed diffused emission in the red, green, and blue channel after 24 hrs incubation with $1/10^{th}$ concentration of Gd_2O_3 nanocluster (35 mg/ml stock), which demonstrated homogeneous internalized and cytoplasmic accumulation. However, the pathway of cellular internalization of nanoclusters is not explored very well, but few findings from previous research suggested that the involvement of cell-receipted medium form endocytosis is very much responsible for the internalization of prepared nanoclusters. [4,371] This *In-vitro* fluorescence imaging study revealed the efficacy of prepared Gd_2O_3 nanoclusters in bioimaging applications. Additionally, the obtained image illustrates that the cell morphology remains uninfluenced after treatment with the Gd_2O_3 nanocluster, which validated the noncytotoxic nature of Gd_2O_3 nanoclusters

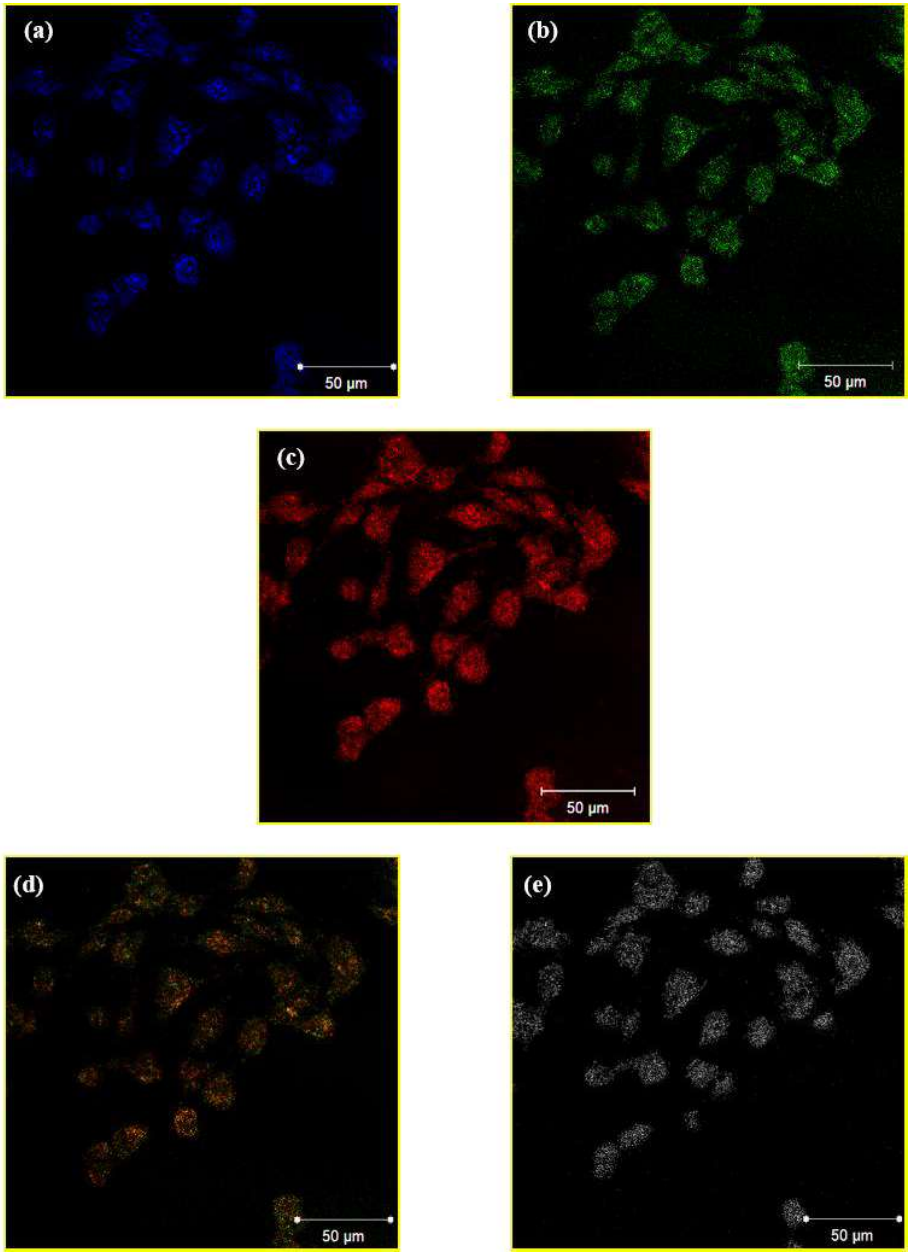

Figure 3.14: Multi-fluorescence confocal image of HaCaT cells treated with Gd_2O_3 nanoclusters (3.5 mg/ml of stock solution), (a) Ex. /Em-366 nm/blue, (b) Ex. /Em-472 nm/green, (c) Ex. /Em-472 nm/red, (d) merged image, (e) Bright-field image.